Korean J. Chem. Eng., 37(10), 1699-1708 (2020)
DOI: 10.1007/s11814-020-0590-6

pISSN: 0256-1115
eISSN: 1975-7220

Fischer-Tropsch Synthesis on Fe-Co-Pt/γ-Al_2O_3 catalyst: A mass transfer, kinetic and mechanistic study

Amir Eshraghi*,†, Ali Akbar Mirzaei*, Rahbar Rahimi, and Hossein Atashi****

*Department of Chemistry, Faculty of Sciences, University of Sistan and Baluchestan, Zahedan, 98135-674, Iran
**Department of Chemical Engineering, Faculty of Engineering, University of Sistan and Baluchestan, P. O. Box 98164-161, Zahedan, Iran
(*Received 27 February 2020 • Revised 10 May 2020 • Accepted 27 May 2020*)

Abstract−Mass transfer limitations and kinetics studies were performed for Fischer-Tropsch Synthesis over spherical 10 wt% Fe-10 wt% Co-0.5 wt% Pt/79.5 wt% γ-Al_2O_3 catalyst in a fixed bed reactor. The external mass transfer limitation was checked by studying the effect of gas hourly space velocity (GHSV) and feed flow rate (at constant GHSV) on CO conversion. Theoretical and practical methods were applied to assess the effect of catalyst pellet size on the internal mass transfer limitation. The results indicated there is external diffusion limitation for GHSV lower than 4,200 h^{-1}. Both the theoretical and practical methods showed that the reaction is free of internal diffusion limitation with average particle sizes of 0.21 and 0.42 mm due to Thiele modulus smaller than 0.4, denoting that the rate of reaction is kinetically controlled. The kinetics results demonstrated the combined enol and carbide mechanism-based model was able to provide a good fit for the experimental data.

Keywords: Fischer-Tropsch Synthesis, Effectiveness Factor, Kinetics Modeling, Spherically-shaped Fe-Co-Pt/γ-Al_2O_3

INTRODUCTION

Rising prices, dwindling reserves of oil, and environmental pollution have resulted in paying great attention to Fischer-Tropsch Synthesis (FTS), which is an alternative route for the production of liquid and gaseous hydrocarbons [1-4]. The reaction is catalyzed by group 8 transition elements, the most common metals of which are iron and cobalt [5,6]. Bimetallic and ternary catalysts are often used more than single metal catalysts in the reaction due to their stability, reducibility, higher activity and change selectivity to a desired product. The effect of Pt on the Co-based catalyst was examined, and the results indicated that the addition of Pt as a promoter has a great impact on the performance and reduction behavior of the catalyst [7-9].

In heterogeneous catalysis, the chemical reaction and the physical phenomenon of mass transfer occur simultaneously; therefore, the results are often not as easy to interpret [10-12]. Mass transfer is classified into external and internal; external mass transfer (film diffusion) is related to the transport of molecules from the gas stream to the catalyst pellets, while internal mass transfer (pore diffusion) is the motion of reactant from the exterior surface into the pores of the catalyst. Mass transfer limitations cause strong concentration gradients that have a negative effect on the achievable productivity and selectivity [13-15]. Under such conditions, the reaction is diffusion limited [16]. Therefore, because of the dependence of kinetics on the mass transfer limitations, external and internal restrictions must be considered and eliminated or minimized in an intrinsic kinetics study, meaning that the kinetics study must be carried out in a chemical reaction-controlled regime [17]. The correct kinetics illustration of the FT reaction is necessary for optimization of the process. Also, a fundamental understanding of the syngas consumption rate or product formation is required to scale up the process. Since the FT reaction network is very complex and involves a large number of reactions, it is very challenging to model the kinetics and product selectivity of this process [18,19]. Many research groups have studied FT kinetics over single or bimetallic catalysts, and several kinetics models have been developed [19-23]. The models have predicted the FT reaction behavior, as well as the distribution of the products under the use of Fe and Co-based catalysts. The kinetic models that have been addressed today range from the simplest based on the power-law formulation to the most complex ones based on the formulation of rigorous reaction mechanisms, such as those of Langmuir-Hinshelwood-Hougen-Watson (LHHW) [24]. These kinetics studies are classified into two classes. In the first, the aim is to describe reaction kinetics based on the rate of reactant consumption, and in the second, the focus is on the FTS product distribution. In both cases, power-law rate expression and mechanistic expressions of LHHW are the general equations for kinetics description of syngas conversion to products [20]. However, no general kinetics model for FT reactions has been reported due to the great dependency of reaction kinetics on operating conditions, pretreatment step, catalyst composition and structural properties [25-27]. To our knowledge, a few kinetics studies have focused on the mass transfer limitations in detail [28-31]. Most of the kinetics studies have used powder catalysts with a size of less than 200 μm and high GHSV (h^{-1}) and have assumed that there are no restrictions.

The main goal of the present study was to derive a kinetic model for the CO hydrogenation on Fe-Co-Pt/γ-Al_2O_3 as a replacement

†To whom correspondence should be addressed.
E-mail: amireshraghi106@gmail.com

active catalyst over a wide range under different reaction conditions. To develop a rate law for the FT reaction, one must make certain that the experimental data are obtained in the absence of restrictions. To check the film diffusion limitation, two types of tests were carried out based on the impact of GHSV and feed flow rate (at constant GHSV) on CO conversion. The pore diffusion limitation was examined by investigating the impact of pellet diameter on the reaction rate using practical and theoretical calculation approaches. Sol-gel/oil-drop and sequential wet-impregnation procedures were used to synthesize γ-alumina support and Fe-Co-Pt/γ-Al_2O_3 catalysts, respectively. Finally, after mass transfer limitations evaluation, collected kinetics data were applied to develop a rate equation that accounts for the CO consumption rate on the γ-Al_2O_3 supported Fe-Co-Pt catalyst. To the best of our knowledge, kinetics and mass transfer studies of FT reaction in a fixed-bed reactor filled with Fe-Co-Pt/γ-Al_2O_3 catalyst have not been carried out so far.

THEORETICAL BACKGROUND

1. Pore Diffusion Limitation

The pore diffusion restriction in the catalyst bed was theoretically studied by calculating the values of Thiele modulus (ϕ). When the Thiele modulus is very small, there would be no limitation of this type [32,33]. The internal mass transfer restriction is commonly more effective than the external for conventional fixed bed reactor [30,33,34]. The well-known Thiele modulus is used to identify the regions of chemical kinetics and mass transfer control. For an *n*th-order reaction within a catalyst pellet it is calculated as:

$$\phi_n = L_p\sqrt{\frac{n+1}{2}\frac{kC_{As}^{n-1}}{D_{eff}}} = \frac{\text{the reaction rate}}{\text{the rate of diffusion}} \quad (1)$$

where n is the reaction order, C_{As}^{n-1} is the concentration for species A at the outer surface of the pellet, k is to the rate constant and D_{eff} is for the effective diffusivity, L_p is the shape factor whose value is related to the catalyst shape, $L_p = \frac{R_p}{3}$ for spherical and $L_p = \frac{R_p}{2}$ for cylindrical pellets. The simplified version of Eq. (1) for a spherical pellet and first-order-reaction at isothermal condition is given as follows:

$$\phi_1 = \frac{R_p}{3}\sqrt{\frac{k}{D_{eff}}} \quad (2)$$

where R_p is the particle radius. The effective diffusivity (D_{eff}) is the combination of Knudsen (D_K) and bulk (D_{AB}) diffusivities that can be calculated using the Bosanquet formula as follows:

$$\frac{1}{D} = \frac{1}{D_{AB}} + \frac{1}{D_K} \quad (3)$$

D_{eff} can be calculated by:

$$D_{eff} = D\frac{\varepsilon}{\tau} \quad (4)$$

where ε and τ are the pellet porosity and tortuosity, respectively. D_{AB} and D_K coefficients were calculated from the equations presented by Hallac [31]. Effectiveness factor (η) is expressed as the measured rate in the pellet divided by the obtained rate in the absence of diffusional effects, and its magnitude ranges from 0 to 1.

$$\eta = \frac{\text{observed rate}}{\text{intrinsic rate}} = \frac{r_{observed}}{r_{intrinsic}} \quad (5)$$

For spherical catalyst pellets and first-order kinetics under isothermal condition, the effectiveness factor is defined as:

Table 1. Elementary reactions set for the reaction in the present study

Model	No.	Elementary reactions	Model	No.	Elementary reactions
FT-I	1	$CO+* \rightleftharpoons CO^*$	FT-II	1	$CO+* \rightleftharpoons CO^*$
	2	$CO^*+* \rightleftharpoons C^*+O^*$		2	$CO^*+* \rightleftharpoons C^*+O^*$
	3	$H_2+2* \rightleftharpoons 2H^*$		3	$H_2+2* \rightleftharpoons 2H^*$
	4	$C^*+H^* \rightleftharpoons CH^*+*$		4	$C^*+H_2 \rightleftharpoons CH_2^*$
	5	$CH^*+H^* \rightleftharpoons CH_2^*+*$		5	$O^*+CO^* \rightleftharpoons CO_2+2*$
	6	$O^*+CO^* \rightleftharpoons CO_2+2*$			
FT-III	1	$CO+* \rightleftharpoons CO^*$	FT-IV	1	$CO+* \rightleftharpoons CO^*$
	2	$H_2+2* \rightleftharpoons 2H^*$		2	$H_2+2* \rightleftharpoons 2H^*$
	3	$CO^*+H^* \rightleftharpoons CHO^*+*$		3	$CO^*+H^* \rightleftharpoons CHO^*+*$
	4	$CHO^*+H^* \rightleftharpoons CHOH^*+*$		4	$CHO^*+H^* \rightleftharpoons C^*+H_2O^*$
	5	$CHOH^*+* \rightleftharpoons CH^*+OH^*$		5	$C^*+H^* \rightleftharpoons CH^*+*$
	6	$CH^*+H^* \rightleftharpoons CH_2^*+*$		6	$CH^*+H^* \rightleftharpoons CH_2^*+*$
	7	$OH^*+H^* \rightleftharpoons H_2O+2*$		7	$H_2O^* \rightleftharpoons H_2O+*$
FT-V	1	$CO+* \rightleftharpoons CO^*$	FT-VI	1	$CO+* \rightleftharpoons CO^*$
	2	$H_2+2* \rightleftharpoons 2H^*$		2	$H_2+2* \rightleftharpoons 2H^*$
	3	$CO^*+H_2 \rightleftharpoons HCOH^*$		3	$CO^*+H_2 \rightleftharpoons HCOH^*$
	4	$CHOH^*+H_2 \rightleftharpoons CH_2^*+H_2O$		4	$CHOH^*+* \rightleftharpoons CH^*+OH^*$
				5	$CH^*+H^* \rightleftharpoons CH_2^*+*$
				6	$OH^*+H^* \rightleftharpoons H_2O+2*$

$$\eta=\frac{3}{\phi}\left(\frac{1}{\tanh\phi}-\frac{1}{\phi}\right) \quad (6)$$

Eq. (6) indicates the dependency of effectiveness factor on Thiele modulus [35]. When the effectiveness factor is very small or the Thiele modulus is large, diffusional resistance limits the rate of reaction; consequently, concentration difference will be observed between the external and internal surfaces of the catalyst pellets [16,36].

The other approach to determine the existence of internal diffusion constraint is using the Weisz-Prater criterion (C_{WP}) shown in the following equation:

$$C_{WP}=\eta\phi^2 \quad (7)$$

The Weisz-Prater criterion or Thiele modulus states that pore diffusion limitation is ignorable when $C_{WP}<0.3$ or $\phi<0.4$ [13,37,38]. It is crucial to eliminate mass transfer restrictions in a kinetics study because their presence leads to an incorrect interpretation of the kinetic data.

2. The Kinetic Model

The rate equation derivation for the reaction is the main part of kinetics modeling and doing this requires a confirmed set of primary steps. According to different mechanisms of FTS, six sets of possible elementary reactions were offered for CO activation mechanism (Table 1). In all mechanistic models, it was proposed that molecular adsorption of CO and H_2 and their dissociation occur on the catalyst active sites. The LHHW and Eley-Rideal (ER) methods were employed to derive the rate law for each proposed mechanism. The following assumptions were used to derive the rate equations: (i) CH_2 monomer was prepared using one CO molecule, (ii) all the active sites on the catalyst are identical types and their total number is constant, (iii) when an elementary reaction is selected as the rate-determining step, other steps are assumed to be quasi-equilibrium, and (iv) the concentrations of adsorbed reactant and its gas phase are in the quasi-equilibrium. All the derived rate expressions are shown in Table 2. Then, the derived models were fitted separately, against experimental data. According to the physico-chemical limitations and statistical tests, the discrimination between the equations was carried out. The derivation of a rate law for FT-IIIRDS4 model is discussed as follows:

$$-r_{CO}=k\theta_{COH}\theta_H \quad (8)$$

where θ_i shows the surface fraction of adsorbed *i* species and k refers to the rate constant. By writing the equilibrium constant for step 3 of FT-III model, θ_{COH} could be calculated as follows:

$$\theta_{COH}=K\frac{\theta_{CO}\theta_H}{C_V} \quad (9)$$

where C_V and K are the concentration of free active sites and the equilibrium constant of step 3, respectively.

$$H_2+2*\underset{k_{des,H_2}}{\overset{k_{ads,H_2}}{\rightleftharpoons}}2H^* \quad (10)$$

$$\begin{aligned}&k_{ads,H_2}P_{H_2}C_V^2-k_{des,H_2}\theta_H^2=0\\&\theta_H=(b_{H_2}P_{H_2})^{0.5}C_V\end{aligned} \quad (11)$$

$$b_{H_2}=\left(\frac{k_{ads,H_2}}{k_{des,H_2}}\right) \quad (12)$$

Table 2. Rate expressions derived for FT reaction on the basis of kinetics models

Model	Rate expression
FT-IRDS4	$-r_{CO}=k\frac{(b_{CO}P_{CO})^{0.5}(b_{H_2}P_{H_2})^{0.5}}{(1+2(b_{CO}P_{CO})^{0.5}+(b_{H_2}P_{H_2})^{0.5})^2}$
FT-IRDS5	$-r_{CO}=k\frac{(b_{CO}P_{CO})^{0.5}b_{H_2}P_{H_2}}{(1+2(b_{CO}P_{CO})^{0.5}+(b_{H_2}P_{H_2})^{0.5})^2}$
FT-IIRDS4	$-r_{CO}=k\frac{(b_{CO}P_{CO})^{0.5}P_{H_2}}{(1+2(b_{CO}P_{CO})^{0.5}+(b_{H_2}P_{H_2})^{0.5})}$
FT-IIIRDS3	$-r_{CO}=k\frac{b_{CO}P_{CO}(b_{H_2}P_{H_2})^{0.5}}{(1+b_{CO}P_{CO}+(b_{H_2}P_{H_2})^{0.5})^2}$
FT-IIIRDS4	$-r_{CO}=k\frac{b_{CO}P_{CO}b_{H_2}P_{H_2}}{(1+b_{CO}P_{CO}+(b_{H_2}P_{H_2})^{0.5})^2}$
FT-IIIRDS6	$-r_{CO}=k\frac{b_{CO}P_{CO}(b_{H_2}P_{H_2})^{1.5}}{P_{H_2O}(1+b_{CO}P_{CO}+(b_{H_2}P_{H_2})^{0.5})}$
FT-IVRDS5	$-r_{CO}=k\frac{b_{CO}P_{CO}(b_{H_2}P_{H_2})^{3/2}}{P_{H_2O}(1+b_{CO}P_{CO}+(b_{H_2}P_{H_2})^{0.5})^2}$
FT-IVRDS6	$-r_{CO}=k\frac{b_{CO}P_{CO}(b_{H_2}P_{H_2})^{2}}{P_{H_2O}(1+b_{CO}P_{CO}+(b_{H_2}P_{H_2})^{0.5})^2}$
FT-VRDS3	$-r_{CO}=k\frac{kb_{CO}P_{CO}P_{H_2}}{(1+b_{CO}P_{CO}+(b_{H_2}P_{H_2})^{0.5})}$
FT-VRDS4	$-r_{CO}=k\frac{b_{CO}P_{CO}(P_{H_2})^{2}}{(1+b_{CO}P_{CO}+(b_{H_2}P_{H_2})^{0.5})}$
FT-VIRDS4	$-r_{CO}=k\frac{b_{CO}P_{CO}P_{H_2}}{(1+b_{CO}P_{CO}+(b_{H_2}P_{H_2})^{0.5})^2}$
FT-VIRDS5	$-r_{CO}=k\frac{b_{CO}P_{CO}b_{H_2}P_{H_2}^2}{P_{H_2O}(1+b_{CO}P_{CO}+(b_{H_2}P_{H_2})^{0.5})^2}$

where b_{H_2} is the adsorption constant of H_2, i^* is the adsorbed *i* species on the catalyst and * represents the free site.

$$CO+*\underset{k_{des,CO}}{\overset{k_{ads,CO}}{\rightleftharpoons}}CO^* \quad (13)$$

$$\begin{aligned}&k_{ads,CO}P_{CO}C_V-k_{des,CO}\theta_{CO}=0\\&\theta_{CO}=b_{CO}P_{CO}C_V\end{aligned} \quad (14)$$

$$b_{CO}=\left(\frac{k_{ads,CO}}{k_{des,CO}}\right) \quad (15)$$

where b_{CO} is the adsorption constant of CO.

$$\begin{aligned}&C_V=1-\sum_{i=1}^{n}\theta_i=1-(\theta_{CO}+\theta_H)=1-(b_{CO}P_{CO}C_V+(b_{H_2}P_{H_2})^{0.5}C_V)\\&C_V=\frac{1}{(1+b_{CO}P_{CO}+(b_{H_2}P_{H_2})^{0.5})}\end{aligned} \quad (16)$$

Finally, the rate equation (FT-IIIRDS4) is derived by substituting

final form of Eqs. (9) and (11) into Eq. (8):

$$-r_{CO\text{-}IIIRDS4}=k\frac{b_{CO}P_{CO}b_{H_2}P_{H_2}}{(1+b_{CO}P_{CO}+(b_{H_2}P_{H_2})^{0.5})^2} \quad (17)$$

3. Kinetic Parameters Estimation and Optimization Methodology

The parameters appearing in the equations listed in Table 2 were estimated out using the Levenberg-Marquardt algorithm. The value of kinetics parameters in the models was obtained by fitting the experimental results. The values of R-Squared and the mean absolute relative residual (MARR) were considered for evaluating the correctness of fits.

$$MARR=\frac{1}{N_{exp}}\sum_{i=1}^{N_{exp}}\left(\frac{\left|r_{i,CO}^{exp}-r_{i,CO}^{mod}\right|}{r_{i,CO}^{exp}}\right)\times 100 \quad (18)$$

$$R^2=1-\frac{\Sigma_{i=1}^{N_{exp}}(r_{i,CO}^{exp}-r_{i,CO}^{mod})^2}{\Sigma_{i=1}^{N_{exp}}(r_{i,CO}^{exp}-\sigma)^2} \quad (19)$$

$$\sigma=\frac{1}{N_{exp}}\left(\sum_{i=1}^{N_{exp}}r_{i,CO}^{exp}\right) \quad (20)$$

where σ is the mean of values of experimental rates.

The dependency of the rate and adsorption constants to temperature can be evaluated through the Arrhenius-type equations (Eqs. (21) and (22)):

$$k=k_0\exp\left(-\frac{E_a}{RT}\right) \quad (21)$$

$$b_i=b_0\exp\left(-\frac{\Delta H}{RT}\right) \quad (22)$$

A well-fitted model must satisfy the following physico-chemical constraints in addition to having appropriate values for the statistical tests:

1. Based on Arrhenius equation, activation energy (E_a) must be positive ($E_a>0$).

2. The heat of adsorption (ΔH) has to satisfy ($-\Delta H>0$) because the syngas adsorption on the catalyst is an exothermic.

Finally, the obtained results over this catalyst were compared with the data reported for FTS kinetics.

EXPERIMENTAL SECTION

1. Spherical γ-Alumina Support Synthesis

The sol-gel/oil-drop procedure was used to prepare γ-alumina. In a typical synthesis, 20 g Al metal was transferred into 100 g deionized water. Under vigorous stirring and approximately constant temperature of 85 °C, HNO_3 solution was gradually added to the above mixture for completely dissolving the aluminum powder. Finally, dense aluminum hydrosol was obtained by heating the mixture at 85 °C for 20 h. Then, an aqueous solution of Hexamethylene tetramine (HMTA, 35 wt%) was added to the hydrosol under vigorous stirring with a volume ratio of 1.5 : 1 at temperature below 10 °C for 20 min. The resulting mixture was placed into a dropper for the injection of droplets into the oil column (height and diameter are 1.60 m and 8 cm, respectively). Immediately after injection, spherical wet-gel granules were obtained owing to the surface tension. Then, the granules were aged in the oil for 8 h at 85 °C and were gathered from the oil column and transferred to an ammonia solution (5 wt%.) at 45 °C for 1.5 h. Subsequently, the spherical white granules were washed with ethanol and deionized water. The washing step was repeated three times to eliminate the oil and ammonia. The washed granules were dried in an oven for 24 h at 45 °C [39]. Finally, the mesopore γ-alumina was prepared by calcination at 650 °C in air in a muffle furnace for 5 h. Different sizes of spherical γ-alumina were prepared by changing the needle diameter.

2. Preparation of γ-Alumina Supported Fe-Co-Pt Catalyst

The ternary 10 wt% Fe-10 wt% Co-0.5 wt% Pt/79.5 wt% γ-Al_2O_3 catalysts were prepared by sequential impregnation approach. The γ-alumina was impregnated by an aqueous solution of iron (III) nitrate nonahydrate, dried at temperature of 50 °C overnight and calcined at 550 °C for 5 h. Then, Co and Pt to Fe/γ-Al_2O_3 catalyst was added by a similar procedure, using a solution of cobalt nitrate and tetra amine platinum (II) nitrate in water, respectively.

3. Characterization Methods

Powder X-ray Diffraction (XRD) spectra of all the samples were recorded using a D8 Advance diffractometer (Bruker AXS, Germany) with CuKα radiation (λ=1.54 Å). The morphology of the prepared support was investigated by scanning electron microscopy (SEM, Tescan Mira III). Surface area and mean pore diameter of catalysts were measured using the Brunauer-Emmett-Teller (BET) method (Quantachrome Nova 2000 automated system, USA).

4. External Mass Transfer Limitation

Two types of tests were performed to study the external diffusion according to our reaction conditions. In the first test, 1.5 g and 6 g of Fe-Co-Pt/γ-Al_2O_3 (diameter 3 mm) catalyst was placed in the reactor and FTS was carried out at (T=260 °C, P=10 bar, H_2/CO=2 and different GHSV=4,800, 4,200, 3,800, 3,200, 2,600, 2,000, 1,600 h^{-1}). In the second method, the reaction was conducted on a catalyst 3 mm in diameter under reaction conditions as follows: reaction temperature (260 °C), total pressure (10 bar), H_2/CO=2 and different feed flow rates proportional to catalyst weight to achieve constant GHSV (4,200 h^{-1}).

5. Internal Diffusion

The presence of pore diffusion limitation was studied by changing the catalyst pellet diameter, while GHSV, feed flow rate and catalytic bed volume were constant. The reaction was performed at (T=260 °C, P=10 bar, H_2/CO=2 and GHSV=4,200 h^{-1}) using eight catalyst samples with the different diameters from 0.2 to 3 mm. The obtained data were used to practical and theoretical investigation of pore diffusion limitation.

6. Kinetics Study

After mass transfer assessment, to collect kinetics data, the experiments were carried out under different operating conditions in a fixed bed reactor, as briefly described below. 1.5 g ($d_p\leq$0.2 mm) of the catalyst was diluted with silicon carbide (1/4, v/v, mesh particle size 100-140) to reach an isothermal condition and loaded between glass wool to keep the catalyst in place. The reduction step was conducted using a continuous stream of pure H_2 (30 ml/min) at 400 °C and pressure of 2 bar for 10 h. Subsequently, the temperature of the reactor was lowered to 200 °C under an H_2 stream and then CO was added to achieve the desired H_2/CO ratio. Kinet-

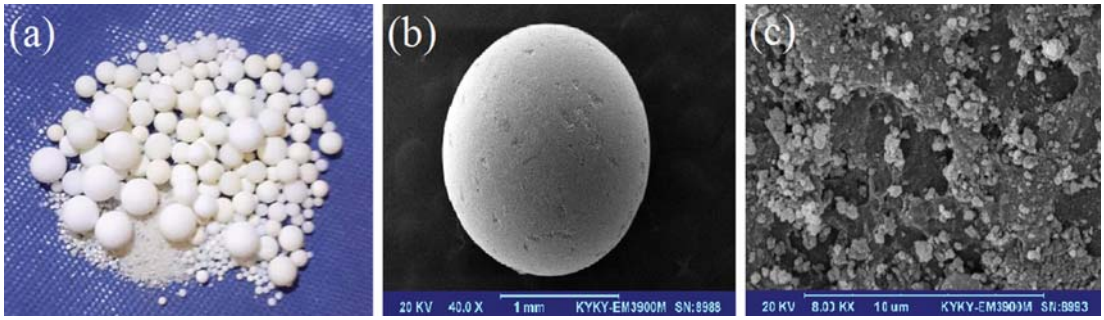

Fig. 1. The optical photograph (a) and SEM micrographs (b), (c) of the spherical γ-Al_2O_3 granules prepared from sol-gel/oil-drop method.

ics experiments were performed at different reaction conditions as follows: (T=220-260 °C, P=2-10 bar, H_2/CO=2, GHSV=4,200 h^{-1}). CO consumption rate is calculated as follows:

$$\frac{W_{cat}}{F^{o}_{CO}} = \int_{X_{CO,in}}^{X_{CO,out}} \frac{dX}{-r_{CO}} \tag{23}$$

The assumption of differential reactor condition can be utilized to calculate the CO consumption rate because CO conversion is low in all kinetics tests. Finally, the rate of reaction is calculated using the following equation:

$$-r_{CO} = \frac{X_{CO} F^{o}_{CO}}{W_{cat}} \tag{24}$$

where X_{CO}, F^{o}_{CO} and W_{cat} are CO conversion, molar flow rate of CO (mol·min^{-1}) and catalyst weight (g), respectively.

RESULTS AND DISCUSSION

1. Catalyst Characterization

The sol-gel/oil-drop method was used to prepare the white spherical granules of γ-Al_2O_3 with different sizes. During the production process of the granules, the operating parameters played critical roles in the properties of the final product [40,41]. Fig. 1(a) shows the optical photograph of the γ-alumina sphere with different sizes. The picture displays granules with high sphericity and uniform size for each diameter of calcined alumina. To obtain more detail about the surface of synthesized spherical alumina, an SEM image of the prepared single granule in this work is shown in Fig. 1(b) and (c). As indicated in Fig. 1(b) and (c), the obtained γ-alumina granule is clearly revealed a spherical particle with a smooth surface and does not have any cracks or other imperfections. The white spherical γ-Al_2O_3 granules were applied as supporting materials to the synthesis of ternary Fe-Co-Pt catalyst for the FTS. X-ray diffraction was used to identify the crystalline phases in the samples. XRD spectra of Al_2O_3 and calcined samples (before and after kinetics tests) are shown in Fig. 2. The XRD diagram of the prepared granules using the oil-drop method indicates characteristic peaks of gamma-alumina (Fig. 2(a)). From the XRD pattern of fresh calcined catalyst (Fig. 2(b)), Co_3O_4 (cubic), Fe_2O_3 (cubic) and $CoFe_2O_4$ (cubic) were observed as predominant phases. Co_3O_4 (cubic) and Fe_2O_3 (cubic) phases were identified in the calcined catalyst after the kinetics tests (Fig. 2(c)). In both samples, no diffraction peaks for Pt were found and this may be attributed to high dispersion or

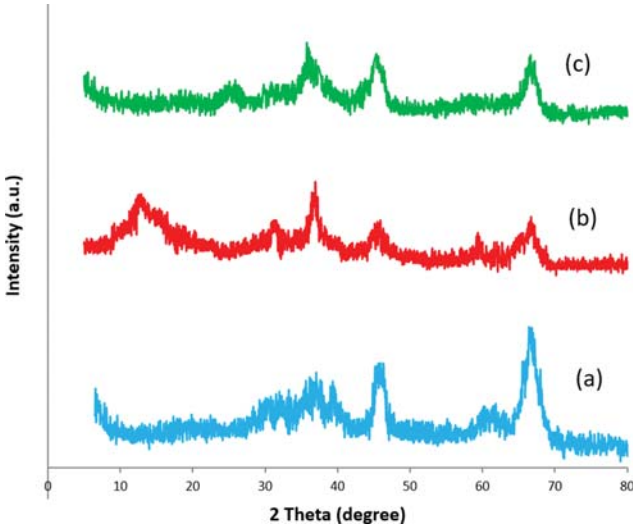

Fig. 2. XRD patterns of the different samples: (a) γ-Al_2O_3 support; (b) calcined Fe-Co-Pt/γ-Al_2O_3 catalyst; (c) spent Fe-Co-Pt/γ-Al_2O_3 catalyst.

Table 3. Physical properties of Fe-Co-Pt/γ-Al_2O_3 (3 mm) catalyst

Parameter	Value
Specific surface area (m^2/g)	272.34
Mean pore diameter (nm)	23.02
Pore volume (ml/g)	0.13
Porosity of catalyst pellet	0.32
Tortuosity of catalyst pellet	6.40

low amount of Pt in the catalysts. Characteristic parameters of the calcined Fe-Co-Pt/γ-Al_2O_3 catalyst (diameter of 3 mm) are shown in Table 3. Based on International Union of Pure and Applied Chemistry (IUPAC) categorization, the catalyst prepared in our study is mesopore [42]. The pore diameter of the obtained catalyst is at least one order of magnitude larger than the diameter of CO molecule (largest reactant). Thus, the catalyst supplied enough porosity for the efficient diffusion of syngas to the interior surface [43].

2. Mass Transfer Limitation

To study the intrinsic kinetics of FTS, the data must be measured in the absence of mass transfer restrictions because they affect

the overall reaction rate. Thus, they must be ascertained and eliminated before the development of the kinetics model. It is a prerequisite that kinetics study must be carried out in the absence of these limitations [28,44,45]. The film diffusion is relevant to the molecule transfer from the gas flow to the proximity of the catalyst pellet. If this step is the slowest process, the external mass transfer will be the reaction rate controller. By examining the impact of GHSV and feed flow rate proportional to catalyst weight to provide constant GHSV on the CO conversion degree, the existence of external diffusion limitation can be investigated. In the first method, the reaction was carried out on 1.5 g and 6 g of spherically shaped Fe-Co-Pt/γ-Al_2O_3 of 3 mm in diameter at operating conditions as follows: T=260 °C, P=10 bar, H_2/CO=2 and different GHSV (4,800, 4,200, 3,800, 3,200, 2,600, 2,000, 1,600 h^{-1}). For the two runs, CO conversion curve versus GHSV is plotted; if the two curves match, film diffusion constraint can be ignored. Fig. 3(a) indicates the diagram related to the effect of GHSV on the CO conversion for assessment of film diffusion limitation. In this figure, region I corresponds to the area where the external diffusion did not limit the reaction rate. Indeed, GHSV=4,200 h^{-1} was selected as the best GHSV for the kinetics experiments. In the second method, FTS was catalyzed by Fe-Co-Pt/γ-Al_2O_3 catalyst of 3 mm in diameter in the reactor under the following conditions: T=260 °C, P=10 bar, H_2/CO=2 and different feed flow rates at constant GHSV=4,200 h^{-1}. In Fig. 3(b), the CO conversion is plotted as a function of feed flow rate at constant GHSV=4,200 h^{-1}, indicating that the conversion was not influenced by increasing feed flow rate at constant GHSV, signifying the absence of film diffusion resistance.

The internal mass transfer is linked to diffusion of reactant from the exterior surface of the pellet into the pores. If this restriction exists, the reaction rate is intraparticle transport controlled. The internal mass transfer limitation was evaluated by investigating the impact of catalyst diameter on the reaction rate. Note that the study must be performed in the absence of film diffusion resistance. After finding the safe GHSV in which film diffusion limitation is ignorable, for the study of pore diffusion limitation, FTS was carried out over eight different sizes of the catalyst (0.2-3 mm) at the same conditions: (T=260 °C, P=10 bar, GHSV=4,200 h^{-1} and H_2/CO=2). The effect of pellet diameter on the rate of reaction was studied using both theoretical calculation (based on the Weisz-Prater criterion or Thiele modulus) and practical approaches. In the theoretical method, the Thiele modulus (ϕ) and Weisz–Prater criterion (C_{WP}) were applied to determine whether or not the reaction is limited by internal diffusion. The values of these two criteria state that pore diffusion limitation is negligible if C_{WP}<0.3 or ϕ<0.4.

Thiele modulus (ϕ) values for all samples were numerically calculated; consequently, Eqs. (6) and (7) were employed to compute η and C_{WP}, respectively. The results are presented in Table 4, where it can be observed that the particle size increase leads to a significant increase in the Thiele modulus. The impact of pore diffusion restriction was not observed for the catalyst diameters up to 0.42 mm, because the values of Thiele modulus for the two average pellet sizes of 0.21 mm and 0.42 mm were less than its limit value. When the reaction is performed on the catalyst size of 0.7 mm and greater than 0.7 mm in diameter, the mass transfer limitations starts and severely limits the reaction, respectively. The dependency of effectiveness factor on Thiele modulus is illustrated in Fig. 4. The value of effective diffusivity (D_{eff}=1.18×10^{-9} $m^2 \cdot s^{-1}$) was calculated

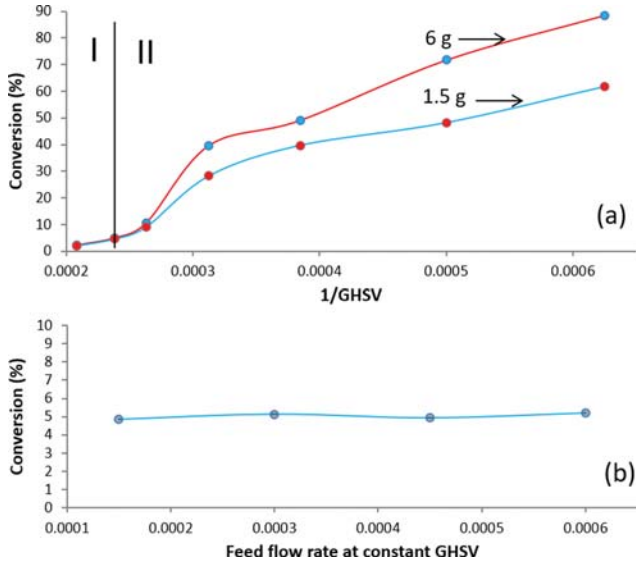

Fig. 3. (a) Relationship between CO conversion and GHSV for two weights of Fe-Co-Pt/γ-Al_2O_3 catalyst (3 mm). In region I, the external diffusion did not limit the reaction rate, while region II refers to the area where the external diffusion limits the reaction rate. (b) CO conversion as a function of feed flow rate at constant GHSV.

Table 4. Results of theoretical investigation of pore diffusion limitation (d_p: Average particle diameter, η: Effectiveness factor, ϕ: Thiele modulus, C_{WP}: Weisz-Prater criterion)

d_p (mm)	η	ϕ	C_{WP}
3.00	0.35	7.50	19.50
2.50	0.37	6.95	17.85
2.00	0.42	5.90	14.70
1.41	0.48	5.05	12.15
1.00	0.81	2.00	3.22
0.70	0.95	0.90	0.77
0.42	0.99	0.35	0.12
0.21	0.99	0.17	0.03

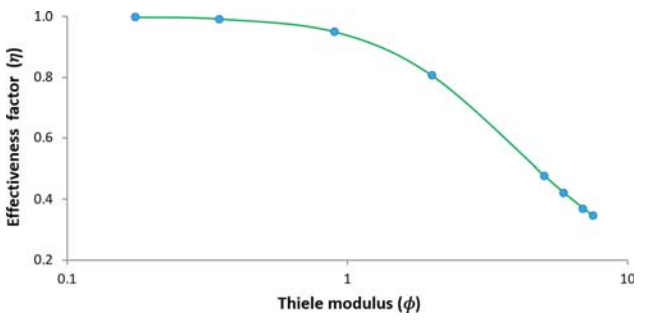

Fig. 4. Effectiveness factor (η) as a function of Thiele modulus (ϕ) for the γ-Al_2O_3 supported Fe-Co-Pt catalyst.

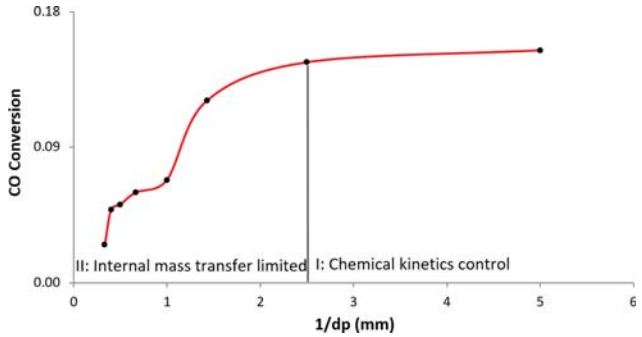

Fig. 5. Experimental method to determine the existence of internal mass transfer limitation.

using Eq. (4). The Weisz-Prater criterion confirmed the accuracy of the investigation of internal diffusion based on Thiele modulus. For the catalyst diameters up to 0.42 mm, the Weisz-Prater number indicates there is no internal mass transfer limitation. In addition to theoretical procedure, the practical technique can give suitable information about internal diffusion regime without any calculation.

In the practical method, at the same reaction conditions and catalytic bed volume, the CO conversion is plotted against the pellet diameter size; a constant CO conversion indicates the restrictions of reaction kinetics only. Hence, based on this view, the FTS was carried out at (T=260 °C, P=10 bar, GHSV=4,200 h^{-1} and H_2/CO=2) over different pellet sizes with the same catalytic bed volume. Fig. 5 shows that in region I CO conversion is independent of catalyst pellet size, whereas in region II, as the particle size increases, the CO conversion decreases, indicating the size dependence of CO conversion. This graph confirms the obtained results based on Thiele modulus. According to both practical and theoretical results, for a catalyst pellet size smaller than 0.7 mm, no concentration gradients exist between the external and the interior surfaces of the catalyst. Based on the above justifications, the mass transfer limitations were neglected; therefore, only the surface reaction is controlling the process. Furthermore, the next kinetics results will show that the reaction rate is not affected by the limitations.

3. Kinetics Study

It is important to make sure of mass transfer limitation absence in the desired reaction conditions before starting up the kinetic investigation [46]. Based on the reported results and justifications in section 4.2., an intrinsic kinetics investigation was conducted at steady state conditions over γ-Al_2O_3 supported Fe-Co-Pt catalyst of 0.2 mm in diameter at (T=220-260 °C, P=2-10 bar, H_2/CO=2, GHSV=4,200 h^{-1}). The operating conditions and results of kinetics tests are presented in Table 5. All the kinetics models in Table 2 were fitted to the experimental data one by one.

FT-III model: The model is based on the combined enol-carbide mechanisms. This is followed by CO adsorption (step 1) and

Table 5. Operating conditions and results for the kinetics experiments with Fe-Co-Pt/γ-Al_2O_3 catalyst (0.2 mm). F^0_{CO} is the molar flow rate of CO, X_{CO} shows CO conversion, r_{CO} represents CO consumption rate

Test no.	Temperature (K)	P_{CO} (bar)	P_{H_2} (bar)	F^0_{CO} (mol·min^{-1})	r_{CO} (mol·min^{-1}·g^{-1})	X_{CO}%
1	493.15	0.63	1.24	3.56E-04	1.77E-05	4.97
2	503.15	0.62	1.24	3.47E-04	1.96E-05	5.65
3	513.15	0.62	1.23	3.39E-04	2.04E-05	6.03
4	523.15	0.60	1.19	3.22E-04	2.89E-05	8.98
5	533.15	0.59	1.17	3.13E-04	3.36E-05	10.85
6	493.15	1.24	2.48	7.07E-04	4.03E-05	5.69
7	503.15	1.22	2.44	6.81E-04	5.02E-05	7.37
8	513.15	1.21	2.42	6.63E-04	5.32E-05	8.02
9	523.15	1.18	2.35	6.33E-04	6.61E-05	10.44
10	533.15	1.17	2.34	6.17E-04	6.81E-05	11.04
11	493.15	1.87	3.73	1.06E-03	5.99E-05	5.65
12	503.15	1.84	3.66	1.02E-03	7.39E-05	7.22
13	513.15	1.81	3.61	9.90E-04	8.40E-05	8.49
14	523.15	1.76	3.52	9.45E-04	1.03E-04	10.88
15	533.15	1.71	3.41	8.98E-04	1.23E-04	13.70
16	493.15	2.50	4.98	1.42E-03	7.73E-05	5.45
17	503.15	2.45	4.88	1.36E-03	1.00E-04	7.38
18	513.15	2.39	4.77	1.30E-03	1.24E-04	9.53
19	523.15	2.32	4.62	1.24E-03	1.52E-04	12.26
20	533.15	2.25	4.48	1.18E-03	1.76E-04	14.93
21	493.15	3.09	6.18	1.76E-03	1.09E-04	6.21
22	503.15	3.05	6.09	1.70E-03	1.28E-04	7.52
23	513.15	2.97	5.92	1.62E-03	1.64E-04	10.12
24	523.15	2.87	5.73	1.54E-03	2.00E-04	13.01
25	533.15	2.79	5.57	1.47E-03	2.27E-04	15.49

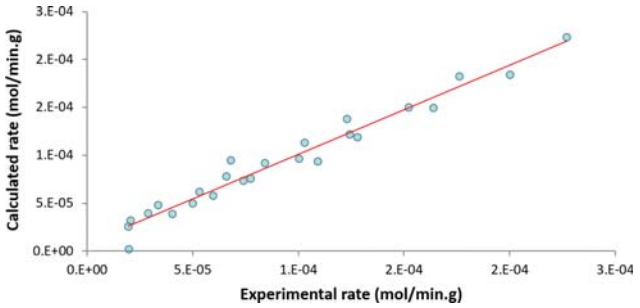

Fig. 6. Comparison between calculated rates versus experimental rates on spherical Fe-Co-Pt/γ-Al_2O_3 catalyst particles 0.2 mm in diameter (operating conditions: T=220-260 °C, P=2-10 bar, GHSV=4,200 h^{-1}, H_2/CO=2).

dissociative adsorption of H_2 (step 2) on the particle surface and then the reaction of adsorbed CO and adsorbed H atom (step 3) to form (-COH) intermediate. -COH hydrogenation (step 4) forms $HCOH^*$ intermediate and then $HCOH^*$ dissociation leads to form CH^* and OH^*. Finally, the reaction of CH^* and H^* results in initiator ($^*CH_2$) formation. The LHHW rate expression ($-r_{CO}=k\frac{b_{CO}P_{CO}b_{H_2}P_{H_2}}{(1+b_{CO}P_{CO}+(b_{H_2}P_{H_2})^{0.5})^2}$) is derived by considering step 4 as RDS.

This was successfully fitted to the experimental data with reasonable accuracy (R^2=0.97 and MARR=5.08%). The parity plot (Fig. 6) compared the experimental rates with the calculated rates for Fe-Co-Pt/Al_2O_3 catalyst. The kinetics and mechanism studies for FTS over Co-, Fe- and Ru-based catalysts show contradicting information regarding the CO dissociation routes. There are two pathways for CO dissociation over a catalyst surface: H-assisted and unassisted (direct) CO dissociation, both of which have been supported by the scientific society. Sonal et al. [19] assumed five different models based on both routes and developed rate laws for each of them. The model based on H-assisted CO dissociation adequately fits their experimental results by considering the formyl formation step as RDS. Zhou et al. [23] reported that CO dissociation on a Fe catalyst surface happens by the H-assisted mechanism. Van der Laan et al. [47] performed FTS kinetics study over Fe-Cu-K and showed that their kinetics data fitted well to the model developed from the enol-carbide mechanism, and the RDS proceeds through hydrogenation of associative adsorbed CO. Inderwildi et al. [48] investigated the CO activation mechanism over cobalt catalyst using density functional theory (DFT) and micro kinetics simulations. They concluded that the carbide is not a dominating mechanism over Co{0001} and that an alternative path via formyl and formaldehyde is preferred. Ojeda et al. [49] studied the mechanism of CO activation over cobalt and iron catalysts. They reported experimental and theoretical evidence showing that the CO dissociation occurs on the surface of both catalysts through H-assisted route. Chun-Fang Huo et al. [50] used spin-polarized DFT to study the mechanism of CO activation on an Fe(111) catalyst. They reported that the dissociation process is catalyzed via formyl (*CHO) intermediate in the presence of H atoms because H-assisted route has a lower barrier than the unassisted route. Azadi et al. [51] performed micro-kinetics analysis of the FTS over a Co/γ-Al_2O_3 catalyst at a Carberry spinning basket batch reactor. They presented a kinetics model based on H-assisted mechanism for FTS over Co/γ-Al_2O_3 catalyst to explain experimental data. On the other hand, some authors also suggested the direct CO dissociation as a dominant mechanism [22,52-55]. However, according to recent reports about CO dissociation over bimetallic catalysts, it can be concluded that CO cannot dissociate alone over catalyst surface [19]. In this study, the kinetics and mechanism of Fischer-Tropsch Synthesis on spherical Fe-Co-Pt/γ-Al_2O_3 catalyst with diameters smaller than 0.2 mm were investigated in the absence of mass transfer limitations. The kinetics equation FT-IIIRDS4 was able to describe laboratory data accurately. The model was developed from the enol/carbide mechanism, where the formation of *HCOH (step 4) was considered as RDS.

Table 6. Value of kinetics parameters for FT-IIIRDS4 model

Kinetics parameters	Value	Units
E_a	80	kJ/mol
$-\Delta H_{CO}$	27.08	kJ/mol
$-\Delta H_{H_2}$	67.76	kJ/mol
k_0	57.02	mol/min·g
b_0^{CO}	0.20	bar^{-1}
$b_0^{H_2}$	14.11	bar^{-1}
R^2	0.97	
MARR	5.08	

4. Estimated Kinetics Parameters

In the estimation process, the best-fitted model not only should provide a good fit of the kinetics data, but also must be consistent with physico-chemical criteria (E_a>0, ΔH<0). The FT-IIIRDS4 kinetics parameters as the best fitted model were estimated using nonlinear regression whose values are given in Table 6. Literature reports a range of 80-110 kJ/mol for the activation energy in the absence of mass transfer limitations [56-59]. For the best fitted model (FT-IIIRDS4), the calculated activation energy for the reaction on alumina supported Fe-Co-Pt ternary catalyst was found to be 80 kJ/mol. This is in agreement with the literature values, confirming the absence of mass transfer restrictions in this study, since in the presence of these restrictions, the activation energy will be about 20-30 kJ/mol [29,35,60]. A range of literature values reported for the heat of hydrogen and carbon monoxide adsorption were −10 to −100 and −20 to −200 kJ/mol, respectively [19,61]. The values obtained for the enthalpy of carbon monoxide and hydrogen adsorption were consistent with those reported for FTS in literature. The prepared catalyst in this study was comprised of three active phases (10wt%Fe-10wt%Co-0.5wt%Pt). Co and Fe-based catalysts are known to be the best metals for application in industrial-scale FTS reactions due to their lowest cost than other active catalysts [62,63]. Also, small amount of Pt was used to improve the reduction temperature and active phase uniformly distribution [64,65]. In addition, the support was prepared by a cheap and more industrial method [39]. Aluminum was used as starting material for support preparation, which is cheaper and more industry-relevant than aluminum alkoxide. Thus, aluminum powder was

used as the precursor. A chlorine-free alumina support can be prepared by using HNO_3 as digestive. Thus, this catalyst could be economically viable for use on industrial scale.

CONCLUSION

The kinetics and mechanism of Fischer-Tropsch Synthesis was comprehensively investigated on 10 wt% Fe-10 wt% Co-0.5 wt% Pt/79.5 wt% γ-Al_2O_3 catalyst by considering the external and internal mass transfer limitations in a fixed-bed reactor. The increase in CO conversion as GHSV decreased showed that film diffusion limitation is limiting the reaction rate for GHSV lower than 4,200 h^{-1}. Both practical and theoretical studies demonstrated the negligible effects of pore diffusion limitation on the rate of reaction for the catalyst pellet size smaller than 0.7 mm due to the effectiveness factor being greater than 95% (ϕ<0.4). Therefore, it was concluded that the FT reaction was performed under the surface reaction rate limited regime. The rate law for CO hydrogenation was derived from the combined carbide and enol mechanism-based model in which H-assisted CO dissociation route occurs on the catalyst surface. The kinetics model was successfully verified with experimental measurements. The activation energy for the model was found to be 80 kJ/mol, which suggests the lack of diffusion restriction.

ACKNOWLEDGEMENTS

The authors gratefully appreciate University of Sistan and Baluchestan for helping and supporting this research.

NOMENCLATURE

b_{CO} : adsorption coefficient of CO
b_{H_2} : adsorption coefficient of H_2
C_{As}^{n-1} : concentration at the external surface of the catalyst pellet
C_{WP} : Weisz-Prater criterion
C_V : concentration of free active sites
D_A : bulk diffusivity [$m^2 \cdot min^{-1}$]
D_{eff} : effective diffusivity [$m^2 \cdot s^{-1}$]
D_K : Knudsen diffusivity [$cm^2 \cdot s^{-1}$]
d_P : pellet diameter [mm]
E_a : activation energy [$kJ \cdot mol^{-1}$]
ER : Eley-Rideal
FTS : Fischer-Tropsch Synthesis
F_{CO}^0 : molar flow rate of CO at the inlet [$mol \cdot min^{-1}$]
GHSV : gas hourly space velocity [h^{-1}]
HMTA : hexamethylene tetramine
IUPAC : international union of pure and applied chemistry
i^* : adsorbed *i* species on the vacant active site
k : reaction rate constant [$mol \cdot g^{-1} \cdot min^{-1}$]
$k_{ads,CO}$: rate constant of adsorption of CO
k_{ads,H_2} : rate constant of adsorption of H_2
$k_{des,CO}$: rate constant of desorption of CO
k_{des,H_2} : rate constant of desorption of H_2
LHHW : Langmuir-Hinshelwood-Hougen-Watson
L_P : shape factor
MARR : mean absolute relative residual
n : reaction order
N_{exp} : number of experiments
P_{CO} : CO partial pressure [bar]
P_{H_2} : hydrogen partial pressure [bar]
R : universal gas constant 8.314 [$J \cdot mol^{-1} \cdot K^{-1}$]
R^2 : coefficient of determination
$-r_{CO}$: consumption rate of CO [$mol \cdot g_{cat}^{-1} \cdot min^{-1}$]
$r_{intrinsic}$: reaction rate in the absence of mass transfer limitations
$r_{observed}$: observed reaction rate
R_P : pellet radius [mm]
RDS : rate determining step
W_{cat} : catalyst weight [g]
X_{CO} : CO conversion

Greek Letters

ΔH : heat of adsorption [$kJ \cdot mol^{-1}$]
ε : pellet porosity
ϕ : thiele modulus
η : effectiveness factor
τ : tortuosity
θ_{CO} : surface occupied with CO
θ_H : surface occupied with H
θ_{COH} : surface occupied with COH
σ : mean of values of experimental rate
* : unoccupied active sites

Superscripts

Exp : experimental value
mod : predicted value

REFERENCES

1. J. H. den Otter, S. R. Nijveld and K. P. de Jong, *ACS Catal.*, **6**(3), 1616 (2016).
2. Y. Xue, J. Sun, M. Abbas, Z. Chen, P. Wang, Y. Chen and J. Chen, *New J. Chem.*, **43**(8), 3454 (2019).
3. M. J. Loedolff, B.-M. Goh, G. A. Koutsantonis and R. O. Fuller, *New J. Chem.*, **42**(18), 14894 (2018).
4. J.-H. Ryu, S.-H. Kang, J.-H. Kim, Y.-J. Lee and K.-W. Jun, *Korean J. Chem. Eng.*, **32**(10), 1993 (2015).
5. B. Sedighi, M. Feyzi and M. Joshaghani, *J. Taiwan Inst. Chem. Eng.*, **50**, 108 (2015).
6. Y. Wang, S. Huang, X. Teng, H. Wang, J. Wang, Q. Zhao, Y. Wang and X. Ma, *Front. Chem. Sci. Eng.*, **14**, 802 (2020).
7. W. Ma, G. Jacobs, R. A. Keogh, D. B. Bukur and B. H. Davis, *Appl. Catal. A: Gen.*, **437-438**, 1 (2012).
8. V. R. Calderone, N. R. Shiju, D. C. Ferré and G. Rothenberg, *Green Chem.*, **13**(8), 1950 (2011).
9. D. Xu, W. Li, H. Duan, Q. Ge and H. Xu, *Catal. Lett.*, **102**(3), 229 (2005).
10. B. J. Lommerts, G. H. Graaf and A. A. C. M. Beenackers, *Chem. Eng. Sci.*, **55**(23), 5589 (2000).
11. H. Bakhtiary-Davijany, F. Dadgar, F. Hayer, X. K. Phan, R. Myrstad, H. J. Venvik, P. Pfeifer and A. Holmen, *Ind. Eng. Chem. Res.*, **51**(42), 13574 (2012).

12. O. Görke, P. Pfeifer and K. Schubert, *Appl. Catal. A: Gen.*, **360**(2), 232 (2009).
13. V. B. Veljković, O. S. Stamenković, Z. B. Todorović, M. L. Lazić and D. U. Skala, *Fuel*, **88**(9), 1554 (2009).
14. H. Becker, R. Güttel and T. Turek, *Catal. Sci. Technol.*, **6**(1), 275 (2016).
15. J. H. Yang, H.-J. Kim, D. H. Chun, H.-T. Lee, J.-C. Hong, H. Jung and J.-I. Yang, *Fuel Process Technol.*, **91**(3), 285 (2010).
16. R. A. Rajadhyaksha and L. K. Doraiswamy, *Catal. Rev.*, **13**(1), 209 (1976).
17. D. M. Marinković, M. R. Miladinović, J. M. Avramović, I. B. Krstić, M. V. Stanković, O. S. Stamenković, D. M. Jovanović and V. B. Veljković, *Energy Convers. Manage.*, **163**, 122 (2018).
18. A. N. Pour, M. R. Housaindokht, J. Zarkesh, M. Irani and E. G. Babakhani, *J. Ind. Eng. Chem.*, **18**(2), 597 (2012).
19. Sonal, K. Kondamudi, K. K. Pant and S. Upadhyayula, *Ind. Eng. Chem. Res.*, **56**(16), 4659 (2017).
20. N. Moazami, M. L. Wyszynski, K. Rahbar, A. Tsolakis and H. Mahmoudi, *Chem. Eng. Sci.*, **171**, 32 (2017).
21. A. Mosayebi and R. Abedini, *Int. J. Hydrogen Energy*, **42**(44), 27013 (2017).
22. T. J. Okeson, K. Keyvanloo, J. S. Lawson, M. D. Argyle and W. C. Hecker, *Catal. Today*, **261**, 67 (2016).
23. L.-P. Zhou, X. Hao, J.-H. Gao, Y. Yang, B.-S. Wu, J. Xu, Y.-Y. Xu and Y.-W. Li, *Energy Fuel*, **25**(1), 52 (2011).
24. C. I. Méndez and J. Ancheyta, *Catal. Today*, In Press (2020).
25. W. Chen, I. A. W. Filot, R. Pestman and E. J. M. Hensen, *ACS Catal.*, **7**(12), 8061 (2017).
26. M. Kaltschmitt and U. Neuling, *Biokerosene: Status and prospects*, Springer-Verlag Berlin Heidelberg, Germany (2017).
27. H. Williams, K. M. Gnanamani, G. Jacobs, D. W. Shafer and D. Coulliette, *Catalysts*, **9**(10), 857 (2019).
28. F. Pöhlmann and A. Jess, *Catal. Today*, **275**, 172 (2016).
29. M. F. M. Post, A. C. Van't Hoog, J. K. Minderhoud and S. T. Sie, *AIChE J.*, **35**(7), 1107 (1989).
30. Y.-N. Wang, Y.-Y. Xu, H.-W. Xiang, Y.-W. Li and B.-J. Zhang, *Ind. Eng. Chem. Res.*, **40**(20), 4324 (2001).
31. B. B. Hallac, K. Keyvanloo, J. D. Hedengren, W. C. Hecker and M. D. Argyle, *Chem. Eng. J.*, **263**, 268 (2015).
32. E. W. Thiele, *Ind. Eng. Chem.*, **31**(7), 916 (1939).
33. D. Vervloet, F. Kapteijn, J. Nijenhuis and J. R. van Ommen, *Catal. Sci. Technol.*, **2**(6), 1221 (2012).
34. O. Levenspiel, *Chemical reaction engineering*, Wiley, New York (1999).
35. J. F. L. Page, *Applied heterogeneous catalysis*, Technip editions, Paris (1988).
36. A. Talebian-Kiakalaieh and N. A. S. Amin, *J. Taiwan Inst. Chem. Eng.*, **59**, 11 (2016).
37. J. Y. Lim, J. McGregor, A. J. Sederman and J. S. Dennis, *Chem. Eng. Sci.*, **141**, 28 (2016).
38. E. E. Gonzo and J. C. Gottifredi, *Catal. Rev.*, **25**(1), 119 (1983).
39. M. Abdollahi, H. Atashi and F. Farshchi-Tabrizi, *Adv. Powder Technol.*, **28**(5), 1356 (2017).
40. Z. Yang and Y. S. Lin, *Ind. Eng. Chem. Res.*, **39**(12), 4944 (2000).
41. G. Buelna and Y. S. Lin, *Micropor. Mesopor. Mater.*, **30**(2), 359 (1999).
42. P. Van Der Voort, C. Vercaemst, D. Schaubroeck and F. Verpoort, *Phys. Chem. Chem. Phys.*, **10**(3), 347 (2008).
43. D. M. Marinković, J. M. Avramović, M. V. Stanković, O. S. Stamenković, D. M. Jovanović and V. B. Veljković. *Energy Convers. Manage.*, **144**, 399 (2017).
44. L. Fratalocchi, C. G. Visconti, L. Lietti, E. Tronconi and S. Rossini, *Appl. Catal. A: Gen.*, **512**, 36 (2016).
45. B. Todic, M. Mandic, N. Nikacevic and D. B. Bukur, *Korean J. Chem. Eng.*, **35**(4), 875 (2018).
46. W. Yu, K. Hidajat and A. K. Ray, *Appl. Catal. A: Gen.*, **260**(2), 191 (2004).
47. G. P. van der Laan and A. A. C. M. Beenackers, *Appl. Catal. A: Gen.*, **193**(1), 39 (2000).
48. O. R. Inderwildi, S. J. Jenkins and D. A. King, *J. Phys. Chem. C*, **112**(5), 1305 (2008).
49. M. Ojeda, A. Li, R. Nabar, A. U. Nilekar, M. Mavrikakis and E. Iglesia, *J. Phys. Chem. C*, **114**(46), 19761 (2010).
50. C.-F. Huo, J. Ren, Y.-W. Li, J. Wang and H. Jiao, *J. Catal.*, **249**(2), 174 (2007).
51. P. Azadi, G. Brownbridge, I. Kemp, S. Mosbach, J. S. Dennis and M. Kraft, *ChemCatChem.*, **7**(1), 137 (2015).
52. F. G. Botes, B. van Dyk and C. McGregor, *Ind. Eng. Chem. Res.*, **48**(23), 10439 (2009).
53. S. Shetty, A. P. J. Jansen and R. A. van Santen, *J. Am. Chem. Soc.*, **131**(36), 12874 (2009).
54. J.-X. Liu, H.-Y. Su, D.-P. Sun, B.-Y. Zhang and W.-X. Li, *J. Am. Chem. Soc.*, **135**(44), 16284 (2013).
55. E. Rebmann, P. Fongarland, V. Lecocq, F. Diehl and Y. Schuurman, *Catal. Today*, **275**, 20 (2016).
56. A. Sari, Y. Zamani and S. A. Taheri, *Fuel Process Technol.*, **90**(10), 1305 (2009).
57. R. Zennaro, M. Tagliabue and C. H. Bartholomew, *Catal. Today*, **58**(4), 309 (2000).
58. A. Einbeigi, H. Atashi, A. A. Mirzaei, H. Zohdi-Fasaei and S. Golestan, *J. Taiwan Inst. Chem. Eng.*, **103**, 57 (2019).
59. H. M. Koo, M. J. Park, D. J. Moon and J. W. Bae, *Korean J. Chem. Eng.*, **35**(6), 1263 (2018).
60. A. Eshraghi, A. A. Mirzaei and H. Atashi, *J. Nat. Gas Sci. Eng.*, **26**, 940 (2015).
61. B. Todic, T. Bhatelia, G. F. Froment, W. Ma, G. Jacobs, B. H. Davis and D. B. Bukur, *Ind. Eng. Chem. Res.*, **52**(2), 669 (2013).
62. J. Li, L. Wu, S. Zhang, J. Wen, M. Liu, C. Wang and X. Li, *Sustain. Energy Fuels*, **3**(1), 219 (2019).
63. J. Li, Y. He, L. Tan, P. Zhang, X. Peng, A. Oruganti, G. Yang, H. Abe, Y. Wang and N. Tsubaki, *Nat. Catal.*, **1**(10), 787 (2018).
64. L. Fratalocchi, L. Lietti, C. G. Visconti, N. Fischer and M. Claeys, *Catal. Sci. Technol.*, **9**(12), 3177 (2019).
65. W. Chu, J. Xu, J. Hong, T. Lin and A. Khodakov, *Catal. Today*, **256**, 41 (2015).